Supplementary Material

Hydrogenation of cinnamaldehyde over palladium nanoparticles supported on functionalized N-doped solid carbon spheres

Alice Magubane[a,b,c], Manoko S. Maubane-Nkadimeng,[a,b,d] and Neil J. Coville[a,b*]

[a] DSI-NRF Centre of Excellence in Strong Materials, University of the Witwatersrand, Johannesburg 2050, South Africa; [b] Molecular Sciences Institute, School of Chemistry, University of the Witwatersrand, Johannesburg 2050, South Africa; [c] Institute of Catalysis and Energy Solutions, University of South Africa, Florida Campus, Johannesburg 1710, South Africa; [d] Microscopy and Microanalysis Unit, University of the Witwatersrand, Johannesburg, South Africa
Email: neil.coville@wits.ac.za

Table of Contents

Characterization of the carbon supports
TEM analysis.....S2
Thermogravimetric analysis.....S2
PXRD and Raman analysis.....S3
BET surface area analysis.....S4
XPS and FTIR analysis.....S4
Characterization of the catalysts
XPS analysis.....S6
TEM analysis of the spent catalysts.....S7

Characterization of the carbon supports

TEM analysis

SCSs were successfully synthesized using a modified Stöber method.[1] Figure S1a shows the TEM image of the RF resin spheres made from resorcinol and formaldehyde polymerization with an average diameter of 820 ± 84 nm (Figure S1c). Annealed SCSs were obtained by carbonizing RF resin spheres at 900 °C under an N_2 atmosphere for 4 h. The obtained annealed SCSs were treated with acid (fSCSs) and are shown in Figure S1b. The TEM images show that the spheres are polydisperse with a diameter ranging between 250-700 nm (Figure S1c). Shrinkage in the diameter of the fSCSs (average diameter = 535 ± 73 nm) compared to the diameter of the RF resin spheres was observed. The shrinkage of the spheres is expected and can be attributed to the loss of both the carbon periphery and the functional groups during carbonization of the RF resin spheres.[2,3] The size of the synthesized spheres was comparable to the spheres reported by Dlamini (565 nm).[1]

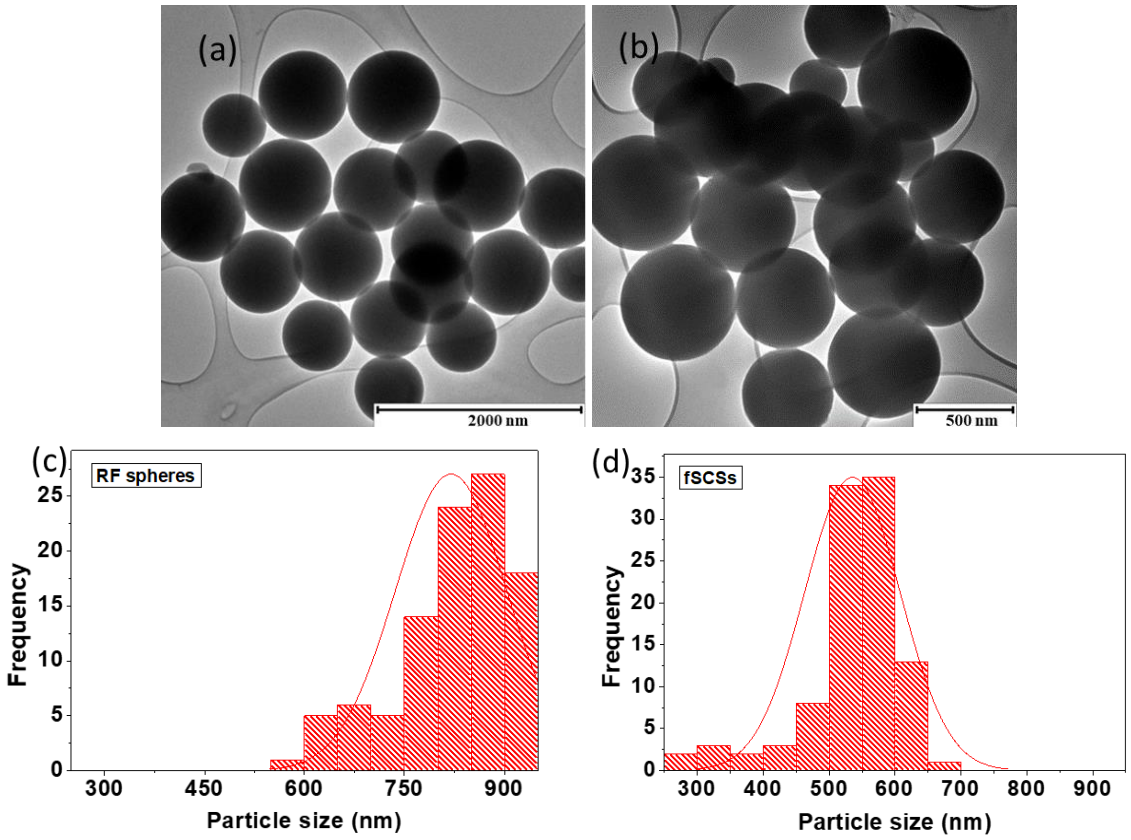

Figure S1. TEM images of (a) RF spheres and (b) fSCSs, and their corresponding (c and d) particle size distributions.

Thermogravimetric analysis

The thermo-oxidative stability of the SCSs and fSCSs was studied in air using the TGA technique. The TGA and the corresponding derivative profiles of the SCSs and fSCSs are shown in Figure S2a and S2b respectively. The acid-treated SCSs were less stable than the parent SCSs. The first derivative peaks below *ca.* 100 °C can be attributed to the loss of moisture. The carbon atoms on the edges of the carbon spheres can react with oxygen upon exposure to air.[4] The derivative peak at *ca.* 241 °C in the DTG profile of the fSCSs can be attributed to the presence and thus thermal removal of the functional groups on the edges of the fSCSs. The calculated weight loss due to the functional groups was estimated to be 7%. The onset of oxidative degradation of the SCSs was

at *ca.* 420 °C whereas the fSCSs started to degrade at *ca.* 368 °C. The last derivative peaks at ~ 653 and 608 °C for SCSs and fSCSs respectively are associated with the oxidation of graphitic carbon in the core of the SCSs. The shift of the derivative peak of fSCSs to a slightly lower temperature (-45 °C) shows that acid treatment creates defects on the structure of the SCSs resulting in less thermo-oxidatively stable carbon spheres. The TGA profiles show that no residues were left at 900 °C, which confirms that the samples do not have impurities.

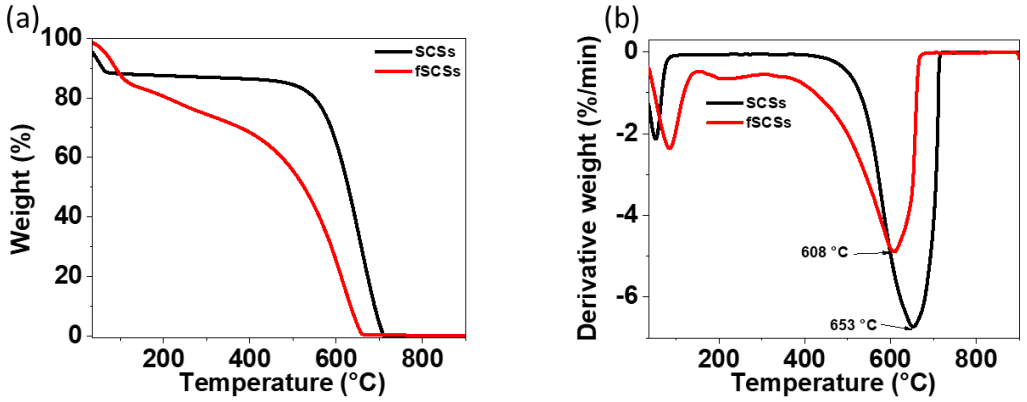

Figure S2. (a) TGA and (b) DTG profiles of SCSs and fSCSs.

PXRD and Raman analysis

The PXRD (Figure S3a) profiles of both SCSs and fSCSs show a broad peak at 24.0° and another peak at 44°. The two peaks were indexed as the (002) and (100) reflections of carbon.[5] The Raman spectra (Fig 3b) of the SCSs and fSCSs show two Raman peaks at (1345 and 1358 cm^{-1}) and (1594 and 1598 cm^{-1}) respectively which correspond to the D and the G bands. The D band is associated with the defects in the carbon structure.[6,7] The G band is associated with stretching of the C-C bond in the sp^2 graphitic domain.[6,7] The intensity ratio of the D and G bands was used to estimate the degree of graphitization in the carbon structure and was estimated to be 1.02 and 0.96 for the SCSs and fSCSs respectively. Acid treatment of SCSs created more defects in the carbon structure and as a result, a decrease in the I_D/I_G ratio was observed.

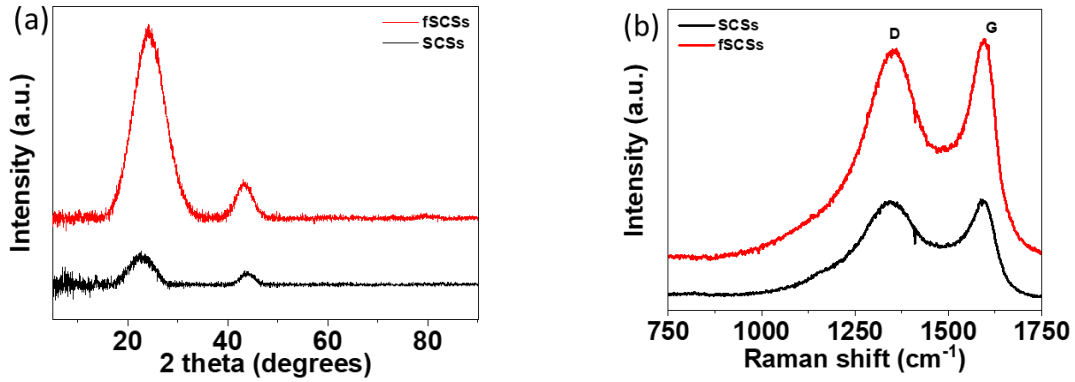

Figure S3. (a) PXRD profiles and (b) Raman spectra of SCSs and fSCSs.

BET surface area analysis

The surface area and the porosity of the carbon spheres were analyzed using nitrogen physisorption. Figure S4 shows the isotherms of the SCSs (a) and fSCSs (b). The results obtained show that acid treatment of the SCSs did not alter the physisorption properties of the carbon spheres as both samples have similar isotherms. The surface properties of the carbon spheres are shown in Table S1. The BET surface area of the SCSs and fSCSs were found to be 557 and 531 m^2/g respectively. The pore size of the carbon spheres remained the same (0.23 nm). The isotherms can be classed as a mixture of type I and IV.[1,8] The data thus indicate that no major structural changes occurred on the SCSs surface after acid treatment.

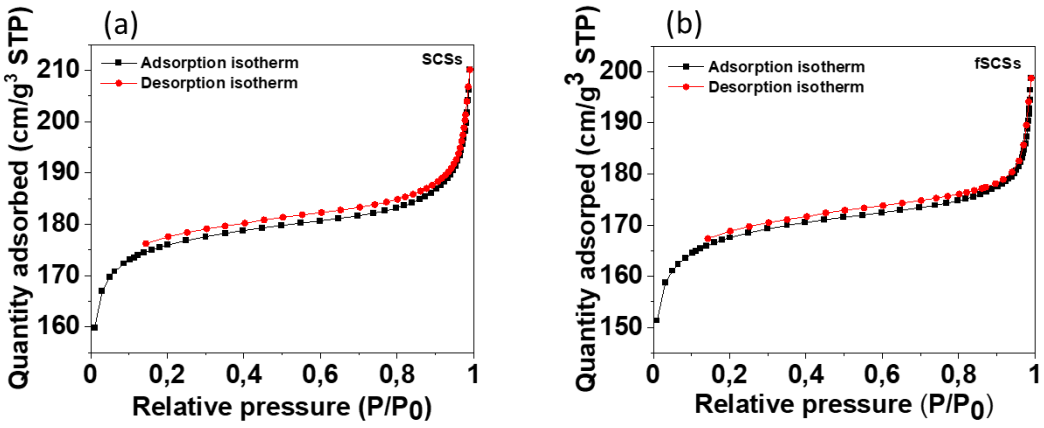

Figure S4. N_2 adsorption-desorption isotherms of the (a) SCSs and (b) fSCSs.

XPS and FTIR analysis

The surface and elemental composition of the fSCSs were analyzed using the XPS technique. The XPS spectra (Figure S5a) shows that the fSCSs are composed of carbon, oxygen, and nitrogen with binding energy of 284.5, 532.2, and 400.1 eV respectively. The atomic % of C1s, O1s, and N1s were determined to be 80.2, 16.8, and 3.0 respectively. The presence of nitrogen can be attributed to the acid treatment of the parent SCSs. Also, Zhao *et al.* proposed that when ammonia solution is used as a catalyst in the RF polymerization it can also act as a nitrogen source.[9] The authors proposed that the N groups were incorporated into the polymer during the RF polymerization. The deconvolution of the C1s XPS spectrum (Figure S5b) of the fSCSs, shows 5 types of carbon species with peaks in the spectrum that correspond to C-C sp^2 (284.2 eV), C-C sp^3 (284.6 eV), C-O (285.8 eV), C=O (288.0 eV), O-C=O (289.2 eV) indicating successful functionalization of the SCSs. The deconvoluted O1s spectra shows two peaks corresponding to C=O (532.7 eV) and C-O (531.3 eV) functional groups.

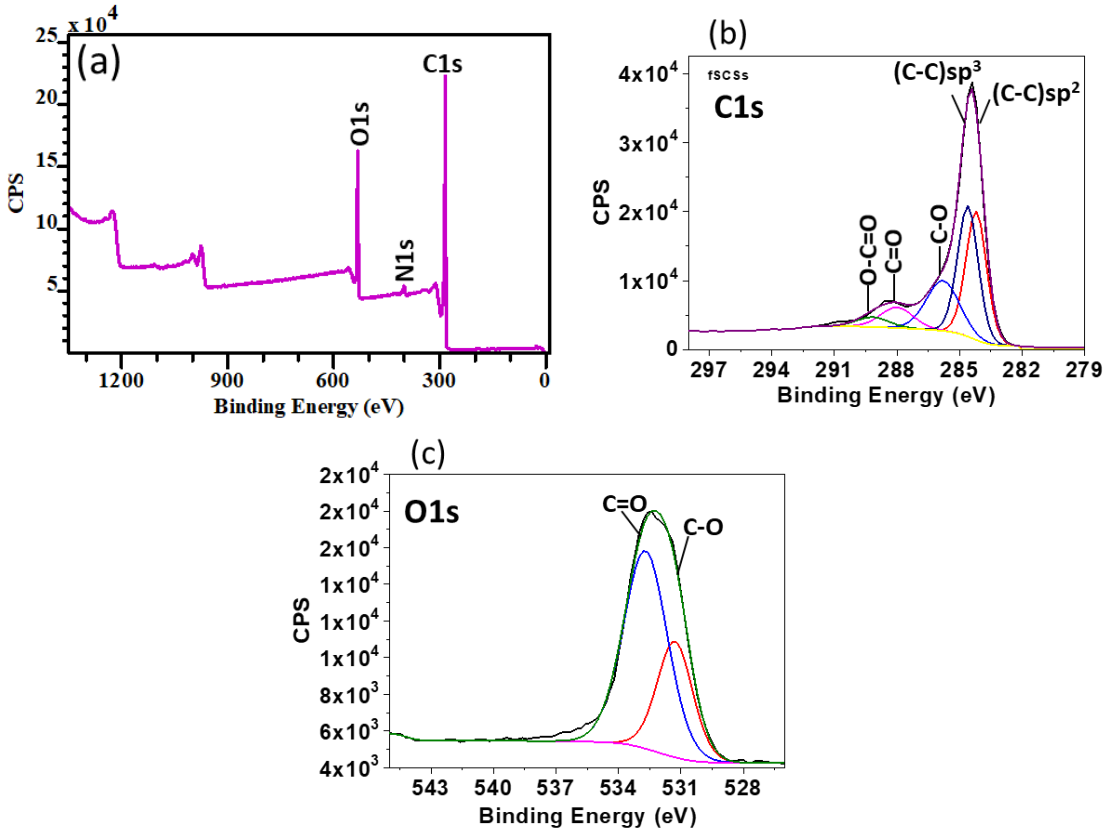

Figure S5. (a) XPS spectra, (b) C1s spectra, and (c) O1s spectra of the fSCSs.

In alignment with the XPS data, FTIR spectroscopy was used to confirm the presence of surface functional groups on the carbon supports. The FTIR spectra (Figure S6) of the CSs, show that the oxygen-containing functional groups become detectable after oxidation with acid. For the SCSs (Figure S6a), the band at 1058 cm^{-1} can be assigned to the stretching mode of the C-O group.[10] The acid-treated SCSs (Figure S6b) show prominent bands at *ca.* 1717 and 1601 cm^{-1} corresponding to the stretching vibrations of C=O from carboxylic functional groups and the C=C stretching mode of aromatic rings.[10–13] The band at 1217 cm^{-1} can be assigned to the stretching mode of the C-O from alcohols or ether functional groups. The band at 3420 cm^{-1} can be assigned to the O-H group from residual water adsorbed on the surface of the CSs and/or to surface carboxyl groups.[13]

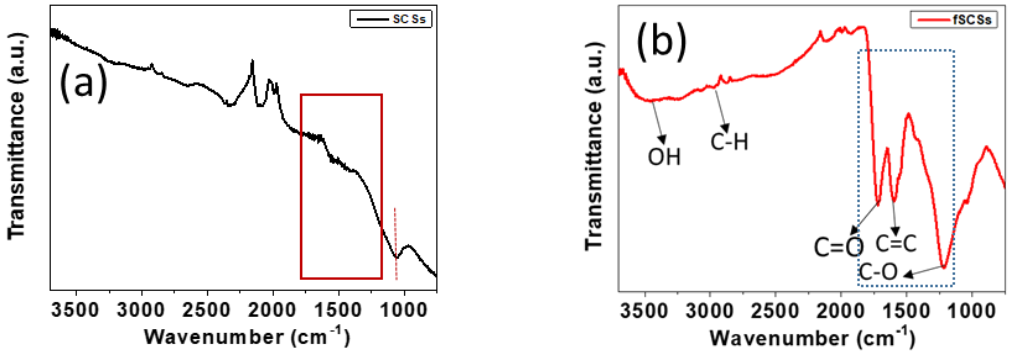

Figure S6. FTIR spectra of the (a) pristine SCSs and (b) functionalized SCSs.

Characterization of the catalysts

XPS analysis

The Pd 3d XPS spectra showed two main peaks corresponding to $3d_{3/2}$ and $3d_{5/2}$ (Figure S7c and S7d). From the deconvolution of the Pd $3d_{5/2}$ peak, it can be noted that the Pd species exists as, Pd (335.2 and 335.0 eV), PdO (336.4 and 336,3 eV), and PdO_2 (337.8 and 337.7 eV) for the Pd/SCSs and Pd/fSCSs. The Pd in the oxide form is due to exposure of the Pd surface to air.[4,14]

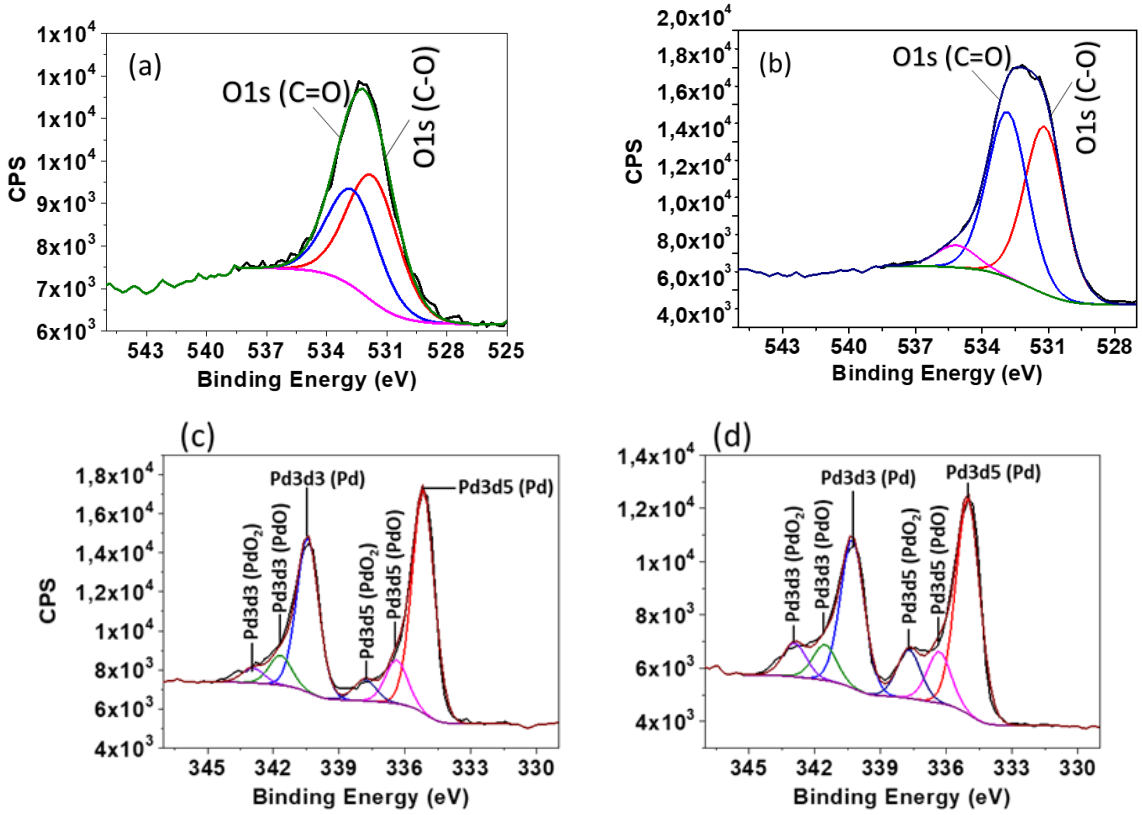

Figure S7. Deconvoluted (a,b) O1s spectra and (c,d)Pd $3d_{5/2}$ spectra of Pd/SCSs and Pd/fSCSs catalyst respectively.

The N content on the Pd/SCSs (1.2%) was found to be less than that of the Pd/fSCSs (2.6%) Each peak due to the N could be deconvoluted into peaks associatied with N-pyridinic, N-pyrollic, N-graphitic and N-oxide groups at ca. 398, 399, 410 and 405 eV.

Table S1. Binding energy and % surface content for the N peaks in the Pd/SCSs and Pd/fSCSs (XPS data)

Catalyst	N-Pyridinic	N-pyrollic	N-graphitic	N-oxide
Pd/SCSs	398.0 (0.2%)	-	401.1 (0.6%)	405.5 (0.2%)
Pd/fSCSs	-	399.4 (2.2%)	400.9 (0.5%)	404.8 (0.4%)

TEM analysis of the spent catalysts

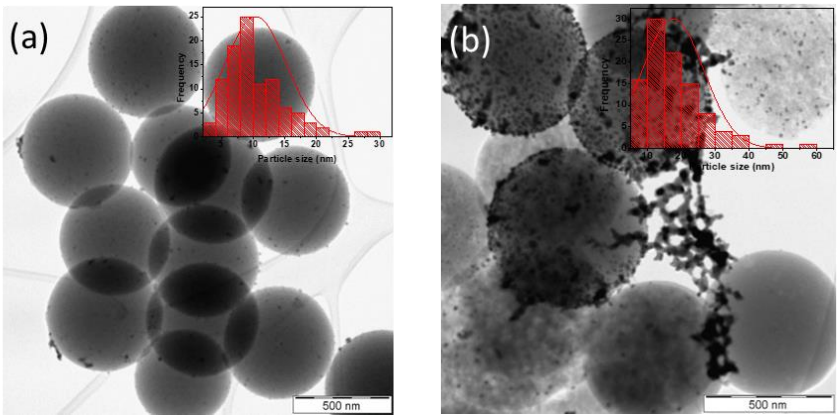

Figure S8. TEM images of the spent catalysts and their corresponding particle size distributions (a) Pd/SCSs and (b) Pd/fSCSs.

References

1. Dlamini, M. W. Ph.D. Thesis, University of the Witwatersrand: Johannesburg, South Africa, 2016.
2. Liu, J.; Qiao, S. Z.; Liu, H.; Chen, J.; Orpe, A.; Zhao, D.; Lu, G. Q. Angew. Chem. **2011**, *123*, 6069. https://doi.org/10.1002/ange.201102011
3. Friedel, B.; Greulich-Weber, S. Small **2006**, *2*, 859. https://doi.org/10.1002/smll.200500516
4. Cattaneo, S.; Sanchez Trujillo, F. J.; Dimitratos, N.; Villa, A. Appl. Sci. **2019**, *9*, 5061. https://doi.org/10.3390/app9235061
5. Pol, V. G.; Shrestha, L. K.; Ariga, K. ACS Appl. Mater. Interfaces **2014**, *6*, 10649. https://doi.org/10.1021/am502324m
6. Ferrari, A. C.; Basko, D. M. Nat. Nanotechnol. **2013**, *8*, 235. http://dx.doi.org/10.1038/nnano.2013.46
7. Ferrari, A. C.; Robertson, J. Phys. Rev. B **2000**, *61*, 14095. https://doi.org/10.1103/PhysRevB.61.14095
8. Sing, K. S. W.; Williams, R. T. Adsorpt. Sci. Technol. **2004**, *22*, 773. https://doi.org/10.1260/0263617053499032
9. Zhao, X.; Zhang, M.; Sun, X.; Li, X.; Li, J. Appl. Surf. Sci. **2020**, *506*, 144591. https://doi.org/10.1016/j.apsusc.2019.144591
10. Jun, L. Y.; Mubarak, N. M.; Yon, L. S.; Bing, C. H.; Khalid, M.; Abdullah, E. C. J. Environ. Chem. Eng. **2018**, *6*, 5889. https://doi.org/10.1016/j.jece.2018.09.008
11. Sezer, N.; Koç, M. Surf. and Interfaces **2019**, *14*, 1. https://doi.org/10.1016/j.surfin.2018.11.001
12. Taklimi, S. R.; Ghazinezami, A.; Askari, D. J. Nanomater. **2019**, *2019*, 1. https://doi.org/10.1155/2019/2836372
13. Ye, B.; Kim, S.-I.; Lee, M.; Ezazi, M.; Kim, H.-D.; Kwon, G.; Lee, D. H. RSC Adv. **2020**, *10*, 16700.

https://doi.org/10.1039/D0RA01665A
14. Sairanen, E.; Karinen, R.; Borghei, M.; Kauppinen, E. I.; Lehtonen, J. ChemCatChem **2012**, *4*, 2055. https://doi.org/10.1002/cctc.201200344